

A SPITZER-SELECTED GALAXY CLUSTER AT $Z=1.62$ ¹

C. PAPOVICH², I. MOMCHEVA³, C. N. A. WILLMER⁴, K. D. FINKELSTEIN², S. L. FINKELSTEIN², K.-V. TRAN², M. BRODWIN⁵,
J. S. DUNLOP⁶, D. FARRAH⁷, S. A. KHAN^{8,9}, J. LOTZ¹⁰, P. MCCARTHY³, R. J. MCLURE⁶, M. RIEKE⁴, G. RUDNICK¹¹
S. SIVANANDAM⁴, F. PACAUD¹², AND M. PIERRE¹³

Accepted for Publication in the Astrophysical Journal

ABSTRACT

We report the discovery of a galaxy cluster at $z=1.62$ located in the *Spitzer* Wide-Area Infrared Extragalactic survey XMM-LSS field. This structure was selected solely as an overdensity of galaxies with red *Spitzer*/IRAC colors, satisfying $([3.6]-[4.5])_{\text{AB}} > -0.1$ mag. Photometric redshifts derived from Subaru XMM Deep Survey (*BViz*-bands), UKIRT Infrared Deep Survey–Ultra-Deep Survey (UKIDSS-UDS, *JK*-bands), and from the *Spitzer* Public UDS survey (3.6–8.0 μm) show that this cluster corresponds to a surface density of galaxies at $z \approx 1.6$ that is $> 20\sigma$ above the mean at this redshift. We obtained optical spectroscopic observations of galaxies in the cluster region using IMACS on the Magellan telescope. We measured redshifts for seven galaxies in the range $z=1.62-1.63$ within 2.8 arcmin (< 1.4 Mpc) of the astrometric center of the cluster. A posteriori analysis of the *XMM* data in this field reveal a weak (4σ) detection in the [0.5–2 keV] band compatible with the expected thermal emission from such a cluster. The color–magnitude diagram of the galaxies in this cluster shows a prominent red-sequence, dominated by a population of red galaxies with $(z-J) > 1.7$ mag. The photometric redshift probability distributions for the red galaxies are strongly peaked at $z = 1.62$, coincident with the spectroscopically confirmed galaxies. The rest–frame ($U-B$) color and scatter of galaxies on the red-sequence are consistent with a mean luminosity–weighted age of 1.2 ± 0.1 Gyr, yielding a formation redshift $\bar{z}_f = 2.35 \pm 0.10$, and corresponding to the last significant star-formation period in these galaxies.

Subject headings: large-scale structure of the universe — galaxies: clusters: general — galaxies: clusters: individual (CIG J0218.3-0510) — galaxies: evolution

1. INTRODUCTION

Galaxy clusters provide important samples to study both the evolution of large–scale structure and the formation of galaxies. The evolution of the number density of massive galaxy clusters involves primarily gravitational physics, which depends strongly on the cosmic mass density, the normalization

and shape of the initial power spectrum, as well as on the dark energy equation of state (e.g., Eke et al. 1998; Bahcall et al. 1999; Borgani et al. 2001; Haiman et al. 2001; Springel et al. 2005; Pacaud et al. 2007; Jee et al. 2009). Because the massive galaxies in clusters formed nearly contemporaneously at $z \gg 1$ with similar star–formation and assembly histories (e.g., Stanford et al. 1998; Tran et al. 2007; Eisenhardt et al. 2008), observations of the evolution of distant cluster galaxies provide strong constraints on hierarchical galaxy evolution models, which make detailed predictions for the formation of these objects (e.g., De Lucia & Blaizot 2007).

Studies of high–redshift clusters have been frustrated by small sample sizes. Few clusters have confirmed redshifts beyond $z \sim 1.3$ (e.g., Mullis et al. 2005; Stanford et al. 2005; Brodwin et al. 2006; Stanford et al. 2006; Eisenhardt et al. 2008; Kurk et al. 2009; Wilson et al. 2009). This dearth of detected galaxy clusters at $z > 1.3$ stems from the significant challenges and potential biases in identifying these structures. Deep X–ray surveys have identified spectroscopically confirmed clusters to $z \lesssim 1.5$ (e.g., Rosati et al. 2004; Stanford et al. 2006), but X–ray selection typically require relaxed systems, which is unlikely to be the case at high redshifts where cluster progenitors will be less massive and more disordered, with less time for the intracluster medium (ICM) to thermalize (e.g., Rosati et al. 2002). Searches for galaxy overdensities around distant radio galaxies require the presence of a massive central galaxy (e.g., Kurk et al. 2000; Miley et al. 2004; Stern et al. 2003; Kodama et al. 2007; Venemans et al. 2007; Zirm et al. 2008; Chiaberge et al. 2010), which may not be an intrinsic property of cluster progenitors.

Other searches utilize the empirically observed, tight color–magnitude relation in central cluster galaxies

¹ This work is based in part on observations made with the Spitzer Space Telescope, which is operated by the Jet Propulsion Laboratory, California Institute of Technology, under NASA contract 1407. This paper also includes data gathered with the 6.5 meter Magellan Telescopes located at Las Campanas Observatory, Chile. This work is based in part on data collected at Subaru Telescope, which is operated by the National Astronomical Observatory of Japan.

² George P. and Cynthia Woods Mitchell Institute for Fundamental Physics and Astronomy, and Department of Physics and Astronomy, Texas A&M University, College Station, TX, 77843-4242; papovich@physics.tamu.edu

³ Observatories, Carnegie Institution of Washington, 813 Santa Barbara St., Pasadena, CA, 91101

⁴ Steward Observatory, University of Arizona, 933 N. Cherry Ave., Tucson, AZ 85721

⁵ W. M. Keck Postdoctoral Fellow, Harvard–Smithsonian Center for Astrophysics, 60 Garden St., Cambridge, MA 02138

⁶ Institute for Astronomy, Royal Observatory, University of Edinburgh, UK

⁷ Astronomy Centre, University of Sussex, Falmer, Brighton, UK

⁸ Pontificia Universidad Católica, Departamento de Astronomía y Astrofísica, 4860 Av. Vicuña Mackenna, Casilla 306, Santiago 22 Chile

⁹ Shanghai Key Lab for Astrophysics, Shanghai Normal University, Shanghai 200234, China

¹⁰ Leo Goldberg Fellow, National Optical Astronomy Observatories, 950 N. Cherry Ave., Tucson, AZ 85719

¹¹ Department of Physics and Astronomy, University of Kansas, 1251 Wescoe Hall Dr., Lawrence, KS, 66045-7582

¹² Argelander Institute for Astronomy, Bonn University, Auf dem Hügel 71, 53121 Bonn, Germany

¹³ Service d’Astrophysique, CEA Saclay, 91191 Gif sur Yvette, France

(the “red sequence”, e.g., Visvanathan & Sandage 1977; Gladders & Yee 2005; Gladders et al. 2007; Kajisawa et al. 2006; Muzzin et al. 2009). However, this selection is biased potentially against clusters whose galaxies have had recent star formation (and overdensities of blue, star-forming galaxies at high redshift have been identified, e.g., Steidel et al. 2005). Most studies of cluster galaxies imply their stellar populations formed at $z_f \gtrsim 1.5$ (e.g., van Dokkum & van der Marel 2007), concurrent with the peak epoch in the star-formation rate density from UV and IR measurements (see e.g., Hopkins & Beacom 2006). As searches for clusters approach the redshift of their formation, cluster galaxies should show increasing indications for star formation with less time available to build up a substantial red-sequence population.

We have initiated a search for galaxy cluster candidates at $z > 1.3$ selected solely as overdensities of galaxies with red [3.6]–[4.5] colors using data from the Infrared Array Camera (IRAC, Fazio et al. 2004) on board *Spitzer* (Werner et al. 2004) following the method of Papovich (2008).¹⁴ At $z < 1$ model stellar populations have blue [3.6]–[4.5] colors because these bands probe the stellar Rayleigh–Jeans tail (with the expectation of some IR-luminous, star-forming galaxies at $z \sim 0.3$ which have a contribution of warm dust to their near-IR colors, see Papovich 2008). At $z \gtrsim 1$ both star-forming and passively evolving stellar populations appear red in [3.6]–[4.5] as these bands probe the peak of the stellar emission at $1.6 \mu\text{m}$ (see Simpson & Eisenhardt 1999; Sawicki 2002; Papovich 2008). Therefore, selecting overdensities of red [3.6]–[4.5] sources potentially identifies high-redshift cluster candidates with little bias from galaxy stellar populations. Papovich (2008) showed that IRAC-selected $z > 1.3$ cluster candidates from the *Spitzer* Wide-Infrared Extragalactic (SWIRE) survey have clustering scale lengths of $r_0 \approx 20 h^{-1}$ Mpc, consistent with other high-redshift galaxy clusters (see Brodwin et al. 2007).

Here we report the discovery and spectroscopic confirmation of a galaxy cluster, ClG J0218.3-0510, (corresponding to *Infrared Cluster* “A”, IRC-0218A, in the 0218-051 field, selected in Papovich 2008), and we discuss its photometric and spectroscopic properties. This galaxy cluster was identified using our IRAC color selection with no other additional criteria imposed. In § 2 we discuss the target selection, and photometric and spectroscopic observations. In § 3 we present the evidence supporting the assertion that this structure is a galaxy cluster, and in § 4 we discuss its properties. In § 5 we summarize our results. Unless otherwise noted we report all magnitudes in reference to the Johnson (1966) magnitude system relative to Vega. We explicitly denote magnitudes relative to the absolute bolometric system (Oke & Gunn 1983) with an AB subscript, $m_{\text{AB}} = 23.9 - 2.5 \log(f_\nu / 1 \mu\text{Jy})$. We use cosmological parameters $\Omega_m = 0.3$, $\Lambda = 0.7$, and $H = 70 \text{ km s}^{-1} \text{ Mpc}^{-1}$ throughout. For this cosmology, the angular diameter distance is $0.5 \text{ Mpc arcmin}^{-1}$ at $z = 1.62$.

2. SAMPLE SELECTION AND SPECTROSCOPIC OBSERVATIONS

2.1. Identification of High-redshift Galaxy Cluster Candidates

We identified galaxy cluster candidates at $z \gtrsim 1.3$ using the IRAC data from the SWIRE survey. These data cover

roughly 50 deg^2 divided over six fields separated on the sky (Lonsdale et al. 2003). We used a simple color selection to identify high-redshift galaxies from *Spitzer*/IRAC 3.6 and $4.5 \mu\text{m}$ photometry. As discussed in Papovich (2008) $>90\%$ of galaxies with $z > 1.3$ have $([3.6] - [4.5])_{\text{AB}} > -0.1 \text{ mag}$. Papovich (2008) identified candidate galaxy clusters at $z > 1.3$ by selecting overdensities of $\gtrsim 30$ objects satisfying this color criterion within radii of $1'.4$ (corresponding to $r < 0.7 \text{ Mpc}$ at $z = 1.5$) from the SWIRE survey data. ClG J0218.3-0510 was identified in Papovich (2008) in the SWIRE XMM-LSS field, and has astrometric coordinates, $\alpha = 2^{\text{h}}18^{\text{m}}21.3^{\text{s}}$, $\delta = -05^{\circ}10'27''$ (J2000), derived from the centroid of the SWIRE IRAC sources in this overdensity. The left panel of figure 1 shows a false-color image using the *B*-band (blue), *i'*-band (green) and $4.5 \mu\text{m}$ image (red) of the field centered on the coordinates of the IRAC-selected overdensity.

2.2. Optical and Near-IR Imaging

The XMM-LSS includes deep optical ($0.4\text{--}1 \mu\text{m}$) and near-IR imaging ($1\text{--}2 \mu\text{m}$) in a portion of the field covering roughly 0.70 deg^2 . Optical imaging is available from the Subaru-XMM Deep Survey (SXDS, Furusawa et al. 2008), obtained with the Subaru Prime Focus Camera (Suprime-Cam) in the broad bandpasses *B*, *R*, *i'*, and *z'*. Near-IR imaging is available from the UKIRT Infrared Deep Sky Survey (UKIDSS, data release 1, Lawrence et al. 2007) ultra deep survey (UDS) in the broad bandpasses *J* and *K*. For the work here, we utilized the *K*-selected catalog of the SXDS and UDS data from Williams et al. (2009). These catalogs reach 5σ -limiting magnitudes in $1''.75$ -diameter apertures of $B_{\text{AB}} < 27.7$, $R_{\text{AB}} < 27.1$, $i_{\text{AB}} < 26.8$, $z_{\text{AB}} < 25.5$, $J_{\text{AB}} < 23.9$, and $K_{\text{AB}} < 23.6 \text{ mag}$. The *K*-selected catalogs also include quasi-total *K* magnitudes, measured in elliptical apertures based on the light profile for each source. For details, we refer the reader to Williams et al. (2009). We corrected the fixed-aperture magnitudes to quasi-total magnitudes using a unique aperture correction for each source, defined as the difference between the fixed aperture and total magnitude derived from the *K*-band for that source, $K(\text{ap}) - K(\text{tot})$. We then applied the aperture correction for each source to its fixed aperture magnitudes measured in the other SXDF and UKIDSS bands.

2.3. Spitzer IRAC Imaging

While the SWIRE IRAC data are sufficient for the selection and study of the galaxies in this cluster, we made use of deeper IRAC imaging in this field from the *Spitzer* public legacy survey of the UKIDSS UDS (SpUDS, PI: J. Dunlop). The SpUDS data cover a field of area 1.5 deg^2 to deeper limiting flux densities than those available with the SWIRE survey data. We measured photometry in $4''$ -diameter apertures in each of the IRAC 3.6, 4.5, 5.8, and $8.0 \mu\text{m}$ images. We applied correction factors of 0.32, 0.36, 0.55, 0.68 mag, respectively, which corrects these aperture magnitudes to total magnitudes for point sources. We matched sources in each of the IRAC-selected catalogs to those in the UKIDSS UDS *K*-selected catalog within $1''$ radii. We combined the “total” aperture-corrected magnitudes for the IRAC data with the aperture corrected photometry for the SXDS and UDS data.

2.4. Photometric Redshifts and the Integrated Redshift Probability

The merged SXDS, UDS, and IRAC catalog covers a wavelength baseline of $0.4\text{--}8 \mu\text{m}$, and we used these data to

¹⁴ Throughout we denote magnitudes measured in the 3.6, 4.5, 5.8, and $7.9 \mu\text{m}$ IRAC channels as [3.6], [4.5], [5.8], and [8.0], respectively.

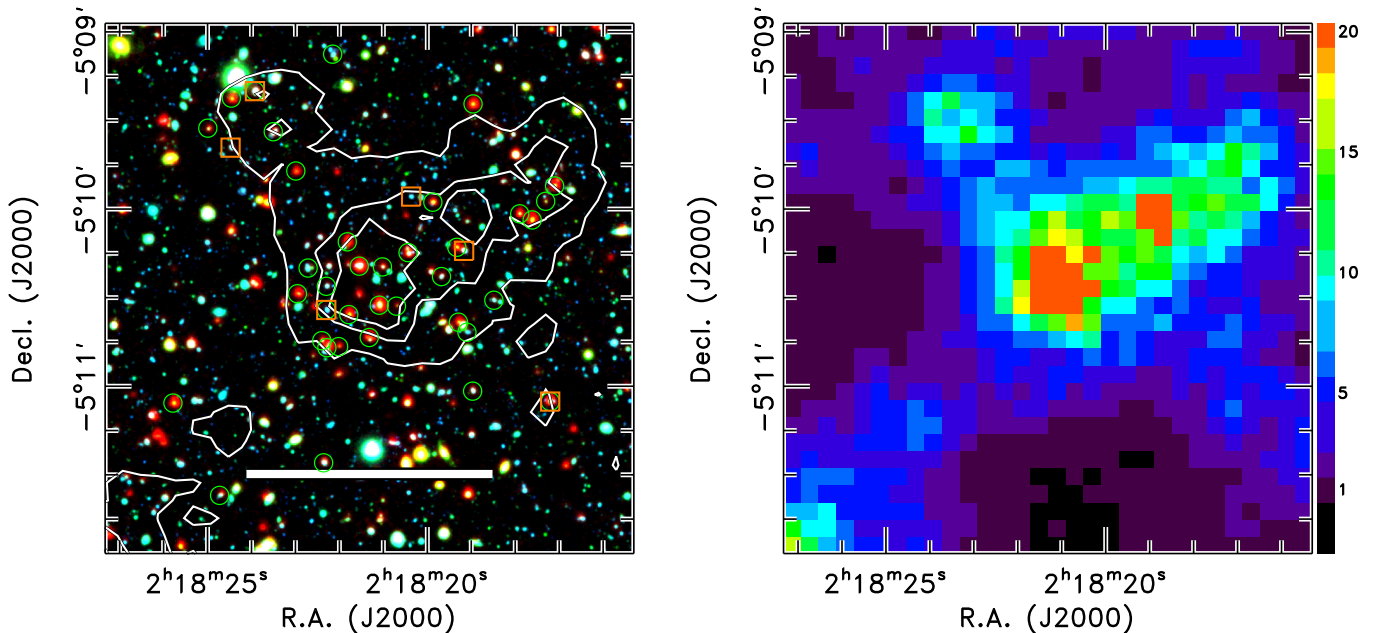


Figure 1. The left panel shows a false-color image of the target field. Blue corresponds to the Suprime-Cam B -band, Green to the Suprime-Cam i -band, and Red to the *Spitzer* $4.5 \mu\text{m}$ band. The images have not been corrected for variations in the data image quality. The image spans $3' \times 3'$, corresponding to $1.5\text{Mpc} \times 1.5\text{Mpc}$ at $z = 1.62$. The heavy white bar shows a distance of 0.7Mpc at the redshift of the cluster. Small green circles denote candidate cluster members with $\mathcal{P}_z > 0.5$ as defined in § 2.4. Orange squares denote those objects with spectroscopically confirmed redshifts $1.62 < z < 1.65$. The contours denote regions with $5, 10,$ and 15σ above the mean density of galaxies with $1.5 < z_{\text{phot}} < 1.7$. The right panel shows the surface density of galaxies with $1.5 < z_{\text{phot}} < 1.7$ in units of the number of standard deviations (σ) above the mean density, ranging from -1 to 20 (as indicated in the plot legend).

study the cluster-candidates selected from the SWIRE IRAC data. We derived photometric redshifts for each source in the K -selected catalog using EAZY (Brammer et al. 2008). We used the default galaxy spectral energy distribution templates with a K -band prior based on the luminosity functions of galaxies in a semi-analytic simulation. We derived the most likely photometric redshift as well as the full photometric-redshift probability distribution function, $P(z)$, normalized such that $\int P(z)dz = 1$ when integrated over all redshifts. Our comparisons against the spectroscopic redshifts in the SpUDS field (Yamada et al. 2005; Simpson et al. 2006; van Breukelen et al. 2007, 2009, C. Simpson, in preparation) showed that the most likely photometric redshifts have uncertainties of $\Delta([z_{\text{sp}} - z_{\text{ph}}]/[1 + z_{\text{sp}}]) = 0.04$ derived from the normalized median absolute deviation (Beers et al. 1990) for the more than 200 galaxies (excluding broad-line AGN) with spectroscopic redshifts in the range $1.0 \leq z \leq 2.0$.

To increase the efficiency of our spectroscopic observations, we computed the surface density of galaxies in the SpUDS field in coarse redshift intervals, and we prioritized those IRAC-selected cluster candidates (selected over the much larger SWIRE field) that corresponded also to large overdensities in photometric redshift. To measure the surface density of galaxies, we divided galaxies into redshift intervals, $\Delta z = 0.2$, and measured the angular distance from each object to the seventh-nearest neighbor, d_7 , and then computed the corresponding surface density, $\Sigma_7 \propto (d_7)^{-2}$. We tested other definitions for the nearest neighbor, which produced similar results (changing the definition of the N th-nearest neighbor changed primarily the angular resolution of the surface density map). We then calculated the mean and standard deviation of the surface density across the entire UDS field.

CIG J0218.3-0510 appears as a strong overdensity of galaxies with $1.5 < z_{\text{ph}} < 1.7$. Figure 1 (right panel) shows the

surface density of galaxies in this photometric-redshift range centered on the IRAC-selected overdensity CIG J0218.3-0510. The color shading corresponds to the number of standard deviations above the mean surface density of galaxies at this redshift over the UDS field. CIG J0218.3-0510 corresponds to a $> 20\sigma$ surface density of galaxies in this redshift interval.

Many of the galaxies in the field of CIG J0218.3-0510 have photometric redshifts centered tightly around $z_{\text{ph}} \simeq 1.6$. We quantified the likelihood of galaxies being associated in redshift by defining the *integrated redshift probability*,

$$\mathcal{P}_z \equiv \int P(z)dz, \quad (1)$$

integrated over $z = z_{\text{cen}} \pm \delta z$. For CIG J0218.3-0510, we used $z_{\text{cen}} = 1.625$ and $\delta z = 0.05 \times (1 + z_{\text{cen}})$ (therefore integrating over $1.49 < z < 1.76$), approximately the 68% confidence range on the photometric redshifts. This was motivated by other cluster-member selection methods using photometric-redshift-selected samples (Brunner & Lubin 2000; Halliday et al. 2004; Eisenhardt et al. 2008; Pelló et al. 2009). Simply defined, the integrated redshift probability is the fraction of the photometric redshift probability distribution function within the redshift intervals (see discussion in Finkelstein et al. 2010). An integrated probability of $\mathcal{P}_z = 0.5$ means that 50% of the integrated photometric redshift distribution lies between $z_{\text{cen}} - \delta z < z < z_{\text{cen}} + \delta z$. The galaxies in the field of CIG J0218.3-0510 with $\mathcal{P}_z > 0.5$ are indicated in figure 1.

2.5. Spectroscopic Observations

We targeted galaxies with high integrated redshift probability in the region of CIG J0218.3-0510 using the *Inamori Magellan Areal Camera and Spectrograph* (IMACS) on the

Table 1
Spectroscopic Redshifts in the ClG J0218.3-0510 Field

| R.A. (J2000) (1) | Decl. (J2000) (2) | \mathcal{P}_z (3) | z (4) | σ_z (5) | R (mag) (6) | Δ ($'$) (7) | r (Mpc) (8) |
|---|-------------------------|------------------------|------------|-------------------|---------------------|----------------------------|---------------------|
| 2 ^h 18 ^m 22.30 ^s | −5°10′34.7 [″] | 0.50 | 1.6224 | 0.0005 | 22.9 | 0.28 | 0.14 |
| 2 ^h 18 ^m 20.37 ^s | −5°09′56.3 [″] | 0.42 | 1.6303 | 0.0012 | 23.6 | 0.57 | 0.29 |
| 2 ^h 18 ^m 19.16 ^s | −5°10′14.7 [″] | 0.47 | 1.6230 | 0.0005 | 23.0 | 0.57 | 0.29 |
| 2 ^h 18 ^m 24.14 ^s | −5°09′45.2 [″] | 0.46 | 1.5356 | 0.0004 | 23.2 | 0.99 | 0.51 |
| 2 ^h 18 ^m 24.48 ^s | −5°09′39.7 [″] | 0.40 | 1.6228 | 0.0005 | 23.4 | 1.12 | 0.57 |
| 2 ^h 18 ^m 17.20 ^s | −5°11′05.7 [″] | 0.61 | 1.6487 | 0.0006 | 23.8 | 1.21 | 0.61 |
| 2 ^h 18 ^m 23.92 ^s | −5°09′20.6 [″] | 0.54 | 1.6222 | 0.0005 | 22.8 | 1.29 | 0.65 |
| 2 ^h 18 ^m 18.92 ^s | −5°08′00.3 [″] | 0.32 | 1.6234 | 0.0013 | 23.7 | 2.52 | 1.28 |
| 2 ^h 18 ^m 17.46 ^s | −5°08′02.2 [″] | 0.48 | 1.4962 | 0.0003 | 22.9 | 2.60 | 1.32 |
| 2 ^h 18 ^m 15.18 ^s | −5°08′11.9 [″] | 0.64 | 1.6224 | 0.0011 | 23.8 | 2.72 | 1.38 |
| 2 ^h 18 ^m 14.50 ^s | −5°06′59.1 [″] | 0.47 | 1.6094 | 0.0008 | 23.5 | 3.86 | 1.96 |

Note. — (1) Right ascension, (2) Declination, (3) Integrated redshift probability, (4) spectroscopic redshift, (5) redshift uncertainty, (6) Suprime-Cam R -band magnitude, (7) angular separation between the galaxy and the cluster astrometric center (see § 2.1), (8) projected physical separation between galaxy and the cluster center for $z = 1.62$.

Magellan/Baade 6.5 m telescope on 2008 Oct 30–31, 2008 Nov 18–19, and again on 2009 Sep 11–12. At the $f/2$ focus IMACS provides multiobject spectroscopic observations over a 27.2′-diameter field of view (FOV), which allowed us to target roughly 100 galaxies in as many as 10 cluster candidates using a single slitmask. We targeted two separate IMACS fields within the UDS, covering 10 cluster candidates in field 1 and 7 in field 2, using two slitmasks per field to alleviate slit collisions. ClG J0218.3-0510 was one of our highest priority targets given the high surface density of objects with high \mathcal{P}_z . The other cluster candidates will be discussed in a forthcoming paper.

We observed with IMACS using the 200 lines/mm grating with the OG570 blocking filter, which provided ~ 7 Å resolution covering 0.6–1 μm . The IMACS CCDs were upgraded in 2008 and have very high red sensitivity, with about a factor of two improvement in sensitivity beyond 8500 Å (A. Dressler 2008, private communication). We used the “nod-and-shuffle” mode (Glazebrook & Bland-Hawthorn 2001) with 1″ × 2.2″ slitlets, which greatly improves the background subtraction and facilitated our spectroscopic redshift success, especially for galaxies at $z > 1.3$. For practical purposes, we prioritized galaxies with $R < 23.3$ mag, but included galaxies to $R < 23.8$ mag (and a few even fainter galaxies). Conditions each night were generally clear, although not photometric, and some time was lost to poor photometric conditions (including most of the time during the 2009 Sept run). Typical image quality during good conditions ranged over 0.6–1″ at full width at half maximum for point sources. Individual exposure times were 1800 s. The total co-added exposure times of data taken under good photometric conditions varied for each mask, and were 3–4 hours on source.

We reduced the IMACS spectroscopic data using the Carnegie Observatories System for MultiObject Spectroscopy (COSMOS, v2.13)¹⁵. The reduction steps to produce 2D spectra include wavelength calibration, bias subtraction, flat fielding, sky subtraction, co-adding the separate frames, and cosmic-ray removal. We extracted 1D spectra at each nod-and-shuffle position separately, as well as the associated uncertainty on the spectra propagated through the reduction

pipeline. We then coadded the individually extracted 1D spectra for each target. We used spectrophotometric standards taken at the end of each night to provide flux calibration. Because photometric conditions varied over the course of each night, our photometric calibration is not absolute (although this does not affect our ability to measure redshifts).

We took spectra of 24 sources with $R < 23.8$ mag, integrated redshift probability $\mathcal{P}_z > 0.3$, and with an angular separation of $\Delta < 4'$ of the astrometric centroid of ClG J0218.3-0510 (corresponding to a physical separation of $r < 2.0$ Mpc at $z = 1.62$). We measured spectroscopic redshifts for 11 of these galaxies, a redshift success rate of about 45% (11/24). These redshifts are listed in table 1. In all cases, the redshifts are secured on the basis of the [O II] emission line. We inspected the 2D reduced data and verified that the emission feature is present in both *independent* spectra obtained from the nod-and-shuffle observation. All of these galaxies were targeted as candidate members of this galaxy cluster. Seven of the galaxies have $1.62 < z < 1.63$ with a mean $\langle z \rangle = 1.622$. Of the remaining galaxies, two have $z = 1.649$ and 1.609 (velocity separations of < 3100 km s^{−1}), and the other two have $z = 1.536$ and $z = 1.496$. Including all nine galaxies within 3100 km s^{−1}, we derive a mean redshift $\langle z \rangle = 1.625$.

Figure 2 shows the one-dimensional spectra for six galaxies with $1.62 < z < 1.65$ with the smallest angular separation ($\Delta < 1.4'$) from the astrometric center of ClG J0218.3-0510. Each spectrum shows the presence of [O II] in emission. Several of the spectra show evidence for interstellar absorption from Mg II and possibly Fe II (one galaxy at $z = 1.649$ shows weak Mg II emission, likely from an AGN).

As the rest of the absorption features are weak, we show in figure 3 a weighted-mean, composite spectrum for the seven galaxies with $1.62 < z < 1.63$, all within $r < 1.4$ Mpc. To construct this spectrum, we scaled each spectrum to the mean flux density in the rest-frame wavelength range 2600–3100 Å. We then weighted each spectrum by the inverse variance using the uncertainty spectrum. The stacked spectrum shows broad features from ~ 3200 –3400 Å, which are artefacts of the stacking procedure. Because we have scaled each spectrum to the mean flux, the fainter galaxies contribute more noise to the stack. These features correlate with strong sky emission, and

¹⁵ <http://obs.carnegiescience.edu/Code/cosmos>

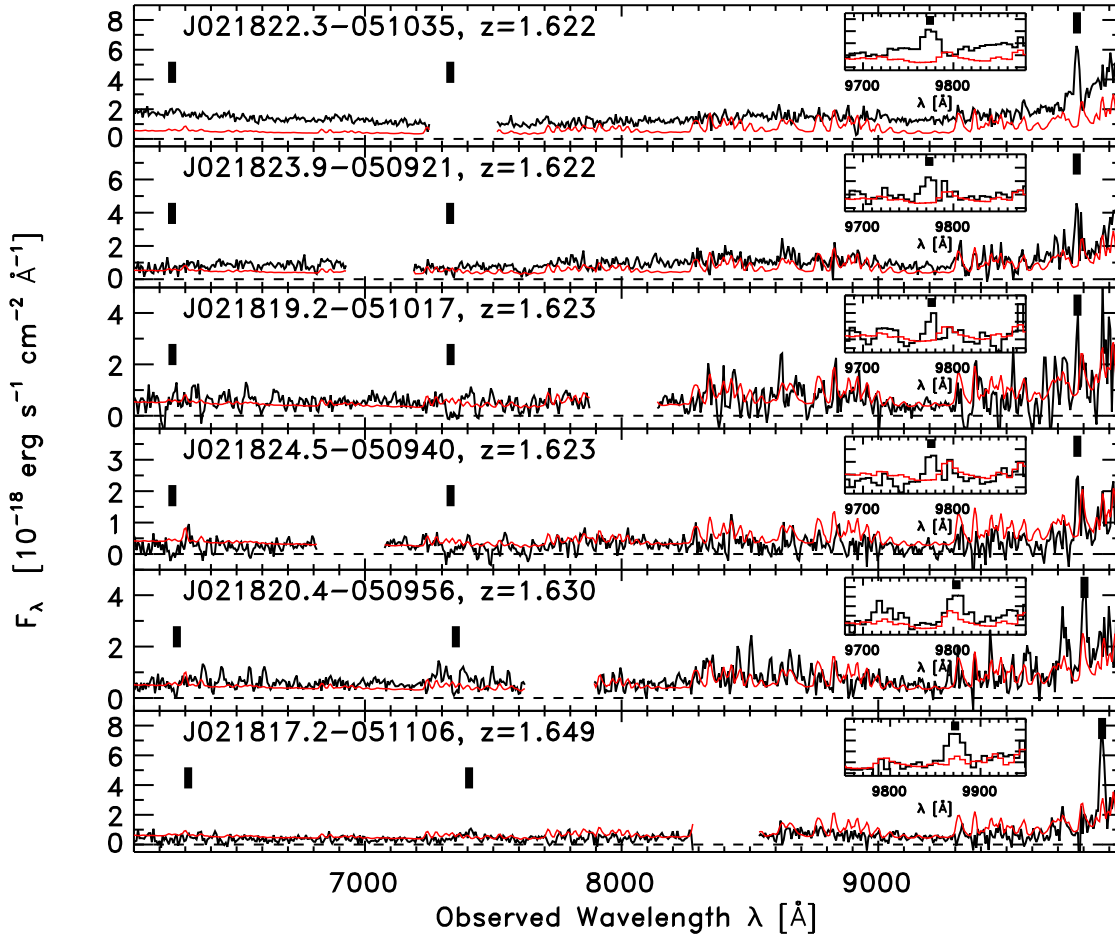


Figure 2. Extracted IMACS spectra for the six galaxies with $1.62 < z < 1.65$ within $1.4'$ of the cluster center (corresponding to $r < 0.7$ Mpc at $z = 1.62$). The inset panel shows the region around $[\text{O II}] \lambda 3727$ at the measured redshift. In all panels, the black line is the measured spectrum. Gaps in the spectra show wavelengths that fall on the “gaps” between the IMACS CCDs. The red line shows the 1σ uncertainties propagated through the data reduction. The thick black lines show the expected locations of $\text{Fe II } \lambda 2374$, $\text{Mg II } \lambda 2800$, and $[\text{O II}] \lambda 3727$ for the measured redshift.

a result of the higher noise in this region of the spectrum. The stacked spectrum shows a strong upturn in flux density at the red end of the spectrum. This feature is unlikely to be intrinsic to the galaxies, and arises from the fluxing uncertainties at the red end of the spectra, due to the decreasing sensitivity of the CCD and the red cut-off of the blocking filter. Nevertheless, strong emission from $[\text{O II}] \lambda 3727$ is observed in the composite spectrum, which is a result of the spectroscopic identification process. The stacked spectrum shows several strong absorption features, in particular $\text{Mg II } \lambda\lambda 2976, 2804$, $\text{Mg I } \lambda 2851$ and absorption from various blends of Fe II lines.

The narrow redshift range of the galaxies in table 1 suggests they are physically associated. Using the spectroscopic redshifts to infer the dynamical conditions of the cluster is dubious because of the unknown dynamical state (see § 4.2). If we assume the galaxies within $< 1500 \text{ km s}^{-1}$ of the mean redshift and within 0.9 Mpc of the astrometric center of the IRAC-selected overdensity sample adequately a virialized structure, then their redshifts correspond to a line-of-sight velocity dispersion of $\sigma = 860 \pm 490 \text{ km s}^{-1}$ using the definition in Carlberg et al. (1996). The uncertainty is derived from a bootstrap resampling of the data (and we make no attempt to remove the additional uncertainty from the redshift errors). However, we further qualify this velocity dispersion because of several biases that likely affect the redshift success rate

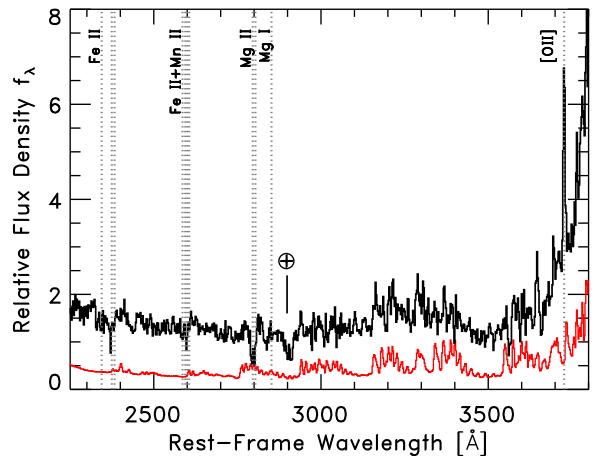


Figure 3. Composite one-dimensional IMACS spectra as a function of rest-frame wavelength for the seven galaxies within $r < 1.4$ Mpc of the astrometric center of CIG J0218.3-0510 with spectroscopic redshifts $1.620 \leq z \leq 1.630$ (see Table 1). The black line shows the composite, weight-averaged spectrum, and the red line is the weighted uncertainty, dominated by emission from the sky. Strong $[\text{O II}]$ is observed, as well as several absorption features, including the doublet $\text{Mg II } \lambda\lambda 2976, 2804$, and absorption from blends of Fe II line. The absorption feature at rest-frame 2900 \AA corresponds to telluric absorption at $\approx 7600 \text{ \AA}$ in the observed frame.

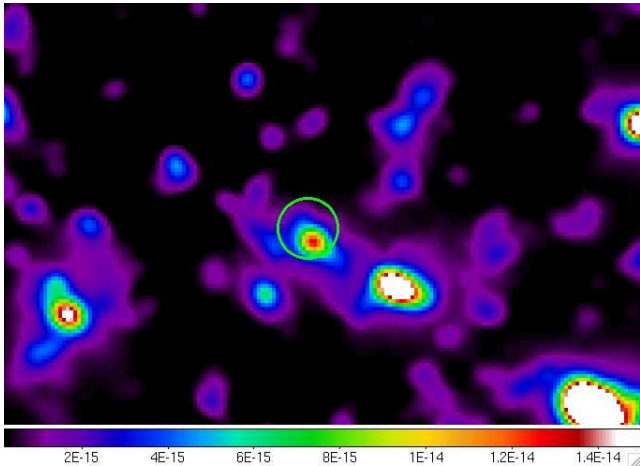


Figure 4. Summed *XMM* image centered on the position of CIG J0218.3-0510. CIG J0218.3-0510 is located on the edges of three adjacent *XMM* positions. The coadded *XMM* data yield an unambiguous source with 4σ significance in the [0.5–2.5] keV band within $10''$ of the position of the cluster. The circle indicates the associated X-ray source and has a diameter of $40''$. The units of the color scale is $\text{erg s}^{-1} \text{cm}^{-2} \text{arcmin}^{-2}$ as indicated by the running bar along the bottom of the image.

for galaxies in this cluster. Firstly, we prioritized only those galaxies with $R < 23.8$ mag for spectroscopy, preferentially excluding fainter galaxies. Second, even with this magnitude criterion, most of the galaxies are faint ($23 < R < 24$ mag) and all the redshift identifications above are based primarily on the [O II] $\lambda 3727$ emission line. At $z = 1.62$ – 1.63 , this line falls at 9780 – 9800 Å, adjacent to a strong sky line at 9800 Å, which hinders the identification of galaxies at $z \approx 1.63$ with emission lines (the only galaxy at this redshift identified above includes strong Mg II absorption). Therefore, our spectroscopic redshifts will be biased against objects at $z \approx 1.63$. If the cluster lies at $z = 1.625$ then roughly half the galaxies with redshifts in the upper end of the distribution will be preferentially missed, biasing the mean redshift and the velocity dispersion measurement. Therefore, while we conclude the galaxies are physically associated as a galaxy (proto-)cluster, we caution against too much interpretation of the dynamics of this cluster using the redshifts above.

2.6. *XMM-Newton* X-ray Imaging

CIG J0218.3-0510 is located within the 1° *XMM* Subaru Deep Field enclosed in the *XMM*-LSS survey (Pierre et al. 2004). While our cluster selection method did not involve X-ray criteria, the presence of diffuse X-ray emission at the cluster location would provide independent confirmation of the existence of a deep gravitational potential well. In a recent analysis of these data Finoguenov et al. (2010) identified two diffuse X-ray sources at distances of $1'8$ and $2'9$ from CIG J0218.3-0510, with redshift estimates of $z = 1.6$ – 1.8 . These may be associated with CIG J0218.3-0510 although their large offset in angular distance challenges this interpretation.

Following our discovery of the close association in redshift of the galaxies in CIG J0218.3-0510, we performed a posteriori analysis of the *XMM* data at the location of this object. CIG J0218.3-0510 is present on three adjacent *XMM* pointings, near the edge of each of them (off-axis values $> 12'$). We coadded the three *XMM* images centered on the position of CIG J0218.3-0510, and applied an adaptive smoothing. The X-ray image is shown in figure 4. The image has an effective

exposure time of $\approx 3 \times 12$ ks at the position of CIG J0218.3-0510. There is an unambiguous source within a radius of $10''$ of the cluster position detected with a 4σ significance. Within a $40''$ -diameter aperture we measured 65 photons ($\pm 30\%$) in the [0.5–2 keV] band. Owing to the low number of photons and the large off-axis position of CIG J0218.3-0510 in the *XMM* images, we are unable to constrain accurately the spatial extent of the X-ray source nor to estimate a gas temperature. However, the detection of the X-ray emission provides an estimate for the virial mass of CIG J0218.3-0510, which we discuss in § 4.2.

3. THE NATURE OF CIG J0218.3-0510

In this section we discuss the evidence that CIG J0218.3-0510 is a galaxy (proto-)cluster. Strictly speaking, a “cluster” is an object that is fully virialized, while a “proto-cluster” is an object that will eventually virialize at later times (lower redshift). It remains to be seen if the dark-matter halo of CIG J0218.3-0510 is fully virialized or if it is still assembling. Nevertheless, we will blur the distinction between these definitions and use the term “cluster” to mean both.

The photometric redshift distributions and spectroscopic redshifts of galaxies in CIG J0218.3-0510 indicate a large overdensity of galaxies at $z = 1.62$ with a high surface density within $r < 0.7$ Mpc. This is illustrated in figure 1. The galaxies with spectroscopic redshifts in this region of high surface density show a preponderance of sources around $z = 1.62$. Furthermore, the IRAC-selected galaxy members of this cluster have high integrated redshift probability as defined in equation 1, implying a high likelihood of being at the cluster redshift. Galaxies with $\mathcal{P}_z > 0.5$ are indicated with circles in figure 1. This includes many red galaxies, which are concentrated near the center of CIG J0218.3-0510 and have very high \mathcal{P}_z values.

Figure 5 shows a montage of photometric redshift probability distribution functions, $P(z)$, for the seven galaxies with the highest integrated redshift probabilities, \mathcal{P}_z , with an angular separation of $\Delta < 1'$ of the cluster center. Without exception these galaxies have red ($z-J$) colors. We targeted several of these galaxies with spectroscopy from IMACS during our 2009 observing run. However, their spectra show only faint optical continua, with no discernible emission features. Nevertheless, while we are unable to derive spectroscopic redshifts for these galaxies, the lack of any emission features is consistent with their photometric redshifts. The photometric redshifts of these galaxies are driven by the strength of the apparent 4000 Å/Balmer break redshifted between the z - and J -bands at $z = 1.62$. As a result, the photometric redshift $P(z)$ functions are sharply peaked at this redshift, and these galaxies have $\mathcal{P}_z > 0.75$, implying that more than 75% of their redshift probability lies between $1.49 < z < 1.76$ with a most likely redshift at $z \approx 1.62$, the mean spectroscopic redshift.

In contrast, the galaxies for which we obtained spectroscopic redshifts have lower \mathcal{P}_z . These galaxies all show [O II] in their spectra, implying relatively recent star formation. Therefore they have weaker 4000 Å/Balmer breaks and subsequently less-well constrained $P(z)$. This is illustrated in figure 5, which shows the $P(z)$ for the seven galaxies with spectroscopic redshifts at that of the cluster. All of these galaxies have bluer ($z-J$) colors, consistent with the evidence of more recent star formation.

The red galaxies in this overdensity dominate the color-magnitude relation for this cluster, similar to the relations observed in clusters at $z \lesssim 1.4$ (e.g., Bower et al. 1992;

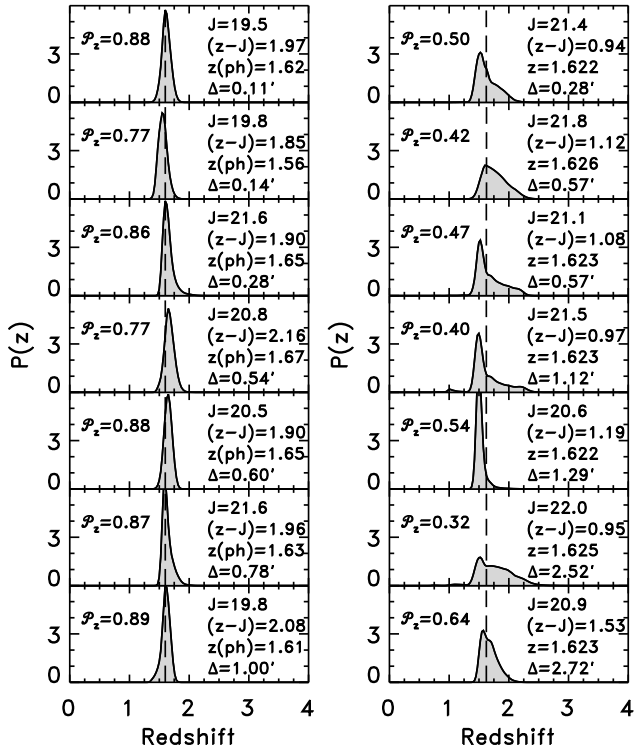


Figure 5. Photometric-redshift probability-distribution functions, $P(z)$, for galaxies in CIG J0218.3-0510. The left figure shows the $P(z)$ for the seven galaxies that have integrated redshift probabilities, $\mathcal{P}_z > 0.75$ with angular separations of $\Delta < 1'$ of the cluster center. Without exception, these galaxies all have very red $(z-J)$ colors. Each panel gives the $(z-J)$ color, J -magnitude, the most likely photometric redshift, the integrated redshift probability, and angular separation from the cluster center. Although these galaxies lack spectroscopic information, their large integrated redshift probabilities support the assertion that they are at the cluster redshift, $z = 1.62$, indicated by the vertical dashed lines. The cluster galaxies with spectroscopic redshifts all show [O II] in their spectra, implying ongoing star formation (see figure 2). They have bluer $(z-J)$ colors and lower values of \mathcal{P}_z , presumably because they have weaker 4000 Å/Balmer breaks owing to the star formation activity. The right figure shows the $P(z)$ for the seven galaxies with spectroscopic redshifts $1.62 < z < 1.63$. Each panel shows the same information as for the left figure, except that they give the spectroscopic redshift instead of the most likely photometric redshift.

Ellis et al. 1997; Stanford et al. 1998; van Dokkum et al. 1998a,b; Blakeslee et al. 2003, 2006; De Lucia et al. 2007; Tran et al. 2007; Lidman et al. 2008; Mei et al. 2009). Figure 6 shows a $z-J$ versus J color-magnitude diagram for all galaxies within 2 arcmin ($r < 1$ Mpc at $z = 1.62$) of the astrometric center of the IRAC-selected overdensity. The z and J bandpasses span the redshifted 4000 Å/Balmer break at redshift $z = 1.62$ providing strong contrast between the cluster galaxies and those in the field. Field galaxies are shown as small data points in figure 6, and these have $\mathcal{P}_z < 0.3$, implying they are foreground or background galaxies. Larger symbol sizes correspond to higher values of \mathcal{P}_z , implying those objects have a greater likelihood of being at the cluster redshift. The cluster galaxies on the red-sequence typically have the highest values of \mathcal{P}_z , especially at the bright end where photometric uncertainties have a smaller effect on the colors. The well-defined color-magnitude relation in CIG J0218.3-0510 is evidence for the cluster-like nature of this object. This is the highest redshift spectroscopically confirmed cluster with such a well-defined red sequence.

The red galaxies that dominate CIG J0218.3-0510 are centrally concentrated, and nearly all are within $\Delta < 1'$ of the cluster center. Very few of the galaxies on the red sequence have angular separations $> 1'$. Of the few that have larger angular separations, most reside within the surface-density contours that extend slightly to the north-east and north-west from the central region (see figure 1). This property of CIG J0218.3-0510 is consistent with the color-density relations observed in other clusters at low and high redshifts (e.g., Dressler 1980; Lidman et al. 2008; Mei et al. 2009) providing further support for the cluster-like nature of CIG J0218.3-0510.

In summary, the spectroscopic and photometric redshifts, the color-magnitude relations, and the surface density-color relations all support the conclusion that CIG J0218.3-0510 is a galaxy cluster. This interpretation is reinforced by the faint X-ray emission measured at the location of this object (see also § 4.2). We therefore conclude these galaxies are physically associated with each other as a cluster, even though we do not have the data to determine if they are fully virialized. In the next section we discuss the properties of this object and the cluster galaxies.

4. DISCUSSION

From the evidence presented above, we conclude that CIG J0218.3-0510 represents a galaxy cluster at $z = 1.62$. Although other candidates for high-redshift galaxy (proto-)clusters at $z > 1.5$ have been reported (e.g., Miley et al. 2004; Brodwin et al. 2007; McCarthy et al. 2007; Zirm et al. 2008; Eisenhardt et al. 2008; Andreon et al. 2009; Kurk et al. 2009; Chiaberge et al. 2010), this is the highest redshift, spectroscopically-confirmed cluster with a strong, well-defined red sequence. While the definition of galaxy “cluster” may be subject to semantics (see above), CIG J0218.3-0510 shows all the characteristics indicative of lower-redshift, rich galaxy clusters.

The fact that CIG J0218.3-0510 has a well-defined red sequence of strongly clustered red galaxies is not a result of the selection method. CIG J0218.3-0510 was selected as an overdensity of galaxies with red IRAC colors (see § 2.1). The IRAC colors at this redshift are blind largely to variations of rest-frame optical colors, and should be sensitive to galaxies with both rest-frame red and blue UV-optical colors (see Papovich 2008). With our full sample, we will compare the properties of CIG J0218.3-0510 against other overdensities of galaxies at this redshift to determine how the galaxies in this object compare to other co-eval (proto-)clusters and to field galaxies.

4.1. Color Evolution and Formation Epoch

As discussed above, CIG J0218.3-0510 is dominated by a strong red sequence of bright galaxies. These are intrinsically very luminous for their redshift, $z = 1.62$. The top axis of figure 6 compares the measured J -band magnitudes to the “characteristic” magnitude, J^* , for the luminosity function of galaxies in the Coma cluster, evolved passively backwards in time to $z = 1.62$ using the model of de Propris et al. (1999). The brightest galaxies in CIG J0218.3-0510 correspond to $J^* - 1$ to $J^* - 1.5$ mag. The descendants of these galaxies at a minimum will be super- L^* cluster galaxies by $z \sim 0$, even without subsequent merging or star formation.

The red galaxy colors imply that they contain older stellar populations. Figure 6 illustrates the expected color of a composite stellar population formed at $z_f = 2.4$ with a

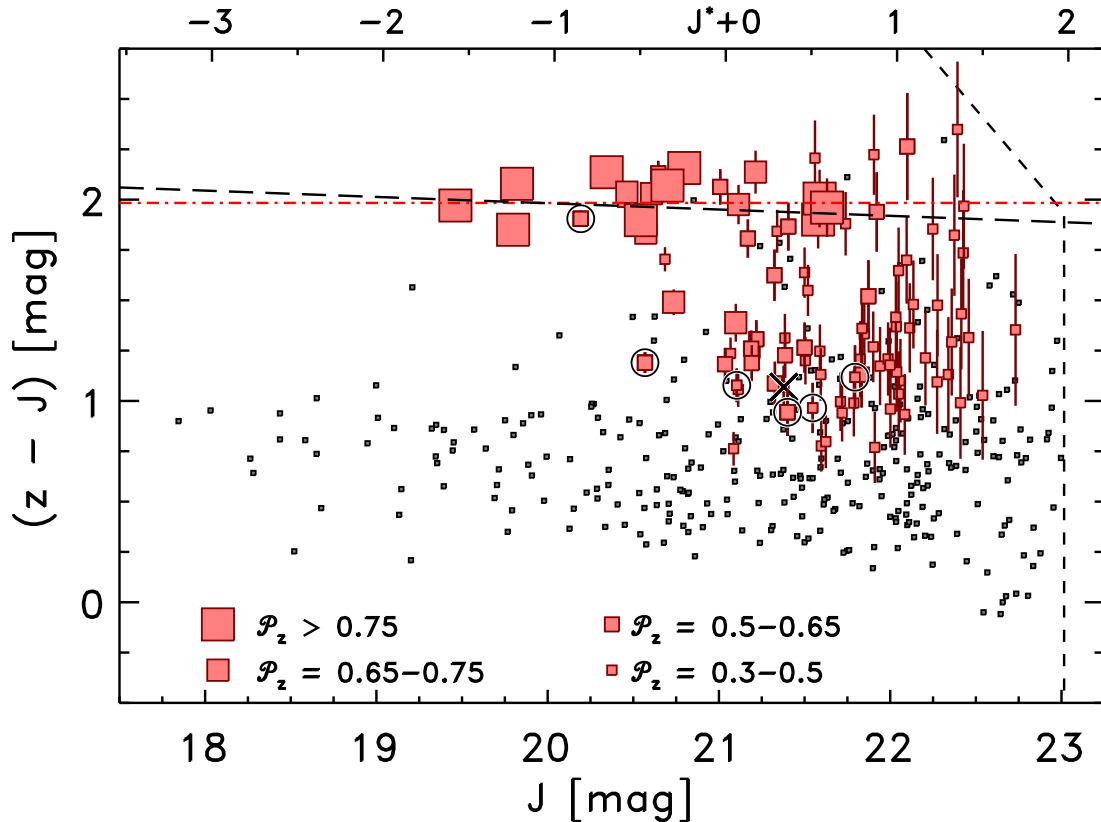


Figure 6. Color–magnitude diagram of all galaxies within $\Delta < 2'$ of the cluster center, corresponding to 1 Mpc at $z = 1.62$. The top axis shows magnitudes in units of J^* , the characteristic luminosity evolved from the measured values for the Coma cluster (de Propris et al. 1999) to $z = 1.62$. The symbol size denotes that likelihood that the galaxy lies at the cluster redshift based on the integrated redshift probability, \mathcal{P}_z , as indicated in the legend. The smallest gray squares all have $\mathcal{P}_z < 0.3$, and are likely foreground or background field galaxies, unassociated with the cluster. Larger, red squares correspond to galaxies with $\mathcal{P}_z > 0.3$, and likely associated with the cluster. The long-dashed line shows a fit to the red sequence (see § 4). The red dot-dashed line shows the expected color of a stellar population observed at $z = 1.62$ formed in a short burst at $z_f = 2.4$ as described in the text. Circles denote those objects spectroscopically confirmed from $1.62 < z < 1.65$. These are bluer galaxies owing to the presence of [O II] emission, facilitating their spectroscopic identification (see § 2.5). The X symbol shows an object with a spectroscopic redshift outside this range. The short dashed lines indicate the 5σ magnitude limits derived for point sources in the imaging data. A strong red–sequence is apparent, which is dominated by galaxies with high \mathcal{P}_z .

star–formation rate that evolves by an e–folding timescale $\tau = 0.1$ Gyr to $z = 1.62$ using the 2007 version of the Bruzual & Charlot (2003) models. This model produces a $(z - J)$ color similar to what we measure for the brighter red galaxies in this cluster (using the Bruzual & Charlot 2003 models produces $z - J$ colors within 0.02 mag for these ages and formation redshift). There is also no indication that ClG J0218.3-0510 contains a population of blue, luminous galaxies. The brightest galaxies within a projected separation of $r < 1$ Mpc of ClG J0218.3-0510 with $(z - J) < 1.5$ mag and $\mathcal{P}_z > 0.3$ have fainter magnitudes, typically sub- J^* . Because the mass–to–light ratios of the stellar populations increase as they redden and fade over time, the dominant population of red–sequence galaxies could not form directly from the less–luminous blue galaxies. Interestingly, the number of red sequence galaxies appears to decline toward the faint end of the red sequence, seemingly at magnitudes well above the detection limit (see figure 6). This observation is similar to the findings of Tanaka et al. (2007), who observed a deficit of red galaxies around a $z = 1.24$ cluster. These results imply a strong evolution in the faint end of the red–sequence luminosity function, extending the relation measured by Rudnick et al. (2009) for moderate redshift clusters to higher redshift. It also appears that there is a lack of faint blue galaxies with $\mathcal{P}_z > 0.3$ but no such lack is seen in the $\mathcal{P}_z < 0.3$ galaxies, indicating

that the photometry is indeed complete to the level indicated in the figure. Further studies of clusters at these redshifts and detailed modeling are needed to confirm this.

The zeropoint, scatter, and slope of the red sequence itself provide constraints on the formation timescales of the galaxies’ stellar populations (e.g., Bower et al. 1992; Aragon-Salamanca et al. 1993). To compare the galaxies in ClG J0218.3-0510 at $z = 1.62$ to those in lower redshift clusters, we converted the observed $(z - J)$ colors to rest–frame $(U - B)$ colors following Mei et al. (2009). We find no evidence for evolution in the slope of the red sequence between ClG J0218.3-0510 and lower redshift galaxy clusters, consistent with the results of other studies (see, e.g., Mei et al. 2009). The top panel of figure 7 shows the rest–frame $(U - B)$ color of ClG J0218.3-0510 and lower redshift clusters taken from the literature at a fixed rest–frame absolute magnitude, $M_B = -21.4$ mag. However, there is strong evolution in the rest–frame $(U - B)$ colors, which become redder with decreasing redshift, consistent with passive evolution. The models in figure 7 illustrate the expected evolution for stellar populations with different formation redshifts ($z_f = 2.0, 2.5, 3.0$, and 5.0), with a star–formation e–folding timescale, $\tau = 0.1$ Gyr, and solar metallicity. The $(U - B)$ color at $M_B = -21.4$ mag for ClG J0218.3-0510 is consistent with stellar populations formed between $2.0 \lesssim z \lesssim 2.5$.

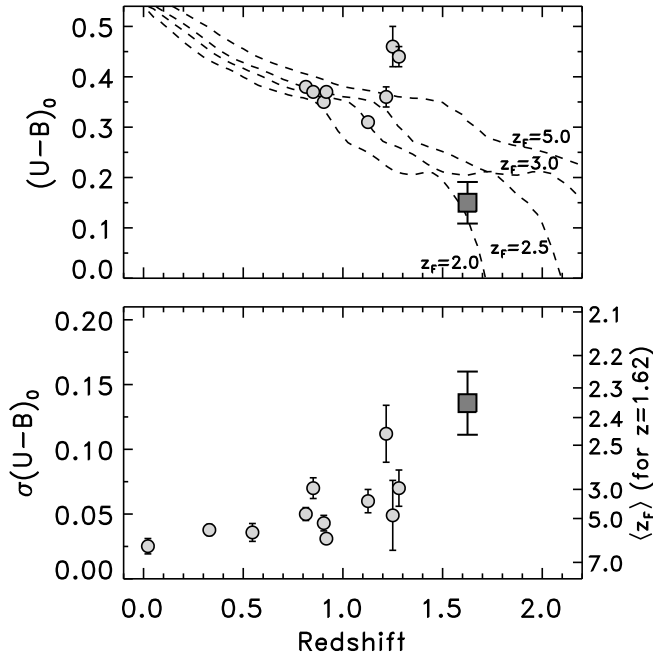


Figure 7. The top panel shows the evolution of the rest-frame $U-B$ color measured at rest-frame $M_B = -21.4$ mag for red-sequence galaxies in clusters as a function of redshift. Smaller circles show the results from lower-redshift clusters (Bower et al. 1992; Ellis et al. 1997; van Dokkum et al. 1998a,b, 2000; Mei et al. 2009). The large box point shows the value derived for the cluster CIG J0218.3-0510 at 1.625 derived here. The curves show the expected evolution of a stellar population with solar metallicity formed with an e-folding timescale $\tau = 0.1$ Gyr at the formation redshift indicated. The bottom panel shows the evolution of the scatter in the rest-frame $U-B$ color for red-sequence galaxies as a function of redshift. Symbols are the same as the top panel. The scatter in the colors of red-sequence galaxies increases with redshift. The right axis of the bottom panel indicates the expected scatter in the rest-frame $(U-B)$ color for a red sequence observed at $z = 1.62$ for a given mean luminosity-weighted formation redshift (see text). The scatter in the $(U-B)$ color for the $z = 1.62$ cluster corresponds to a luminosity-weighted formation redshift of $\bar{z}_f = 2.25-2.45$, consistent with the evolution in the $(U-B)_0$ color.

We model the scatter in the colors of the red-sequence galaxies in CIG J0218.3-0510 by following Hilton et al. (2009, and references therein). We construct a series of composite stellar populations with star-formation e-folding timescale of $\tau = 0.1$ Gyr and solar metallicity. We tested other values for the metallicity (ranging from $0.2 Z_\odot$ and $2.5 Z_\odot$), but found that they did not reproduce simultaneously the zero-point and scatter in the rest-frame $(U-B)$ colors for a consistent formation epoch. In our model each galaxy forms stars in a single burst of star formation that begins at an initial formation redshift, z_F , and lasts for a duration Δt . We allow the duration Δt to vary from $\Delta t = 0$ to a maximum equal to the lookback time from z_F to $z = 1.62$, the redshift at which the cluster is observed. We allow for a range of formation redshift (with a maximum formation redshift taken to be when the lookback time was 4 Gyr), where at each, z_F , we construct a simulated sample of 10^5 galaxies with ages assigned randomly from a uniform distribution with $0 < t < \Delta t$. From these simulated galaxies we compute the scatter in the simulated color distributions and the luminosity-weighted age. Then, for a given measurement of the scatter in the colors, we infer the corresponding luminosity-weighted age and thus obtain an estimate for the formation redshift of the red-sequence

galaxies in the cluster.

We calculated the scatter for the red sequence galaxies in CIG J0218.3-0510, including those galaxies with integrated redshift probability $P_z > 0.3$ within a projected radius of 1 Mpc (2 arcmin) of the cluster center. We used an iterative rejection algorithm to include only red galaxies within 2.5σ of the derived red sequence. We derive the scatter about the median absolute deviation (Beers et al. 1990), which yields $\sigma(U-B) = 0.136 \pm 0.024$. We compare this to the red sequences of other galaxy clusters and our models in the bottom panel of figure 7. There is a marked increase in the scatter in the $(U-B)$ color with redshift, which is expected because the cluster galaxies are observed closer in time to when they formed their stellar populations (e.g., Mei et al. 2009; Hilton et al. 2009). The right axis of the panel indicates the modeled relationship between $\sigma(U-B)$ and the formation redshift, z_f for the model stellar populations observed at $z = 1.62$. The scatter in the rest-frame $(U-B)$ color for CIG J0218.3-0510 corresponds to range of formation redshift, $2.25 \leq z \leq 2.45$, using the 2007 version of the Bruzual & Charlot (2003) stellar population synthesis models (using the 2003 models has a negligible change on the formation redshifts for the stellar population ages involved here). We note that this is an upper limit as we have made no attempt to remove the color measurement uncertainties from the intrinsic scatter. If we have overestimated the scatter, the formation redshift will be *higher*. Given the agreement between the formation epochs derived from the red-sequence zero-point and scatter, we do not think this is a serious effect.

Therefore, both the zero-point and scatter of the rest-frame $(U-B)$ colors for red-sequence galaxies in CIG J0218.3-0510 imply a formation epoch of $z_f \simeq 2.25-2.45$ (a lookback time of 1.0–1.3 Gyr from $z = 1.62$). This corresponds to the last major star-formation episode in these red cluster galaxies. This is a similar formation epoch as found in many studies of other $z > 1$ cluster galaxies (e.g., Mei et al. 2009; Hilton et al. 2009; Rosati et al. 2009), although at least one cluster (XMM J2235.3-2557 at $z = 1.39$) has galaxies with formation epochs ranging from $z_f \sim 2$ to $z_f \sim 6$ (Rosati et al. 2009). The formation epoch of CIG J0218.3-0510 is also consistent with the colors and spectral indices of galaxies in lower-redshift massive clusters (e.g., Stanford et al. 1998; van Dokkum & van der Marel 2007). Furthermore, studies show that a high fraction of massive galaxies at $z > 2$ have high levels of star formation (e.g., Kriek et al. 2006; Papovich et al. 2006), and these are likely consistent with the evolution of the cluster galaxies. These properties all support the conclusion that the galaxies of CIG J0218.3-0510 will become typical galaxies found in rich clusters at later times.

4.2. Dynamical Mass Estimate

As discussed above, it is unclear if the cluster galaxies of CIG J0218.3-0510 sample a virialized, relaxed dark-matter halo, or if this object is in the process of assembling through mergers. Under the assumption that the galaxies are virialized, we use the velocity dispersion to provide a crude estimate for the dynamical mass of CIG J0218.3-0510 as a reference, although we qualify this with the caveats in § 2.5. For a velocity dispersion, $\sigma = 860 \pm 490$ km s⁻¹ (see § 2.5), the corresponding dynamical mass estimate is $M_{\text{dyn}} \sim 3r_{\text{vir}}\sigma^2 \sim 4 \times 10^{14} M_\odot$ for a virial radius of 0.9 Mpc. We derive the same

dynamical mass estimate using M_{200} (Carlberg et al. 1997).¹⁶ Even so, we caution the reader that the dynamical mass may be highly uncertain given the statistical errors and systematic biases.

This mass is a factor of ~ 4 larger than the limiting halo mass of the IRAC-selected clusters (Papovich 2008), and if accurate then it implies that CIG J0218.3-0510 resides in one of the most overdense environments in the SWIRE survey. In this case, based on the expected growth of dark-matter haloes (Springel et al. 2005) the mass of CIG J0218.3-0510 should increase to at least $10^{15} M_{\odot}$ by $z = 0.2$, becoming a rich cluster of galaxies comparable to the Coma cluster.

The high dynamical mass estimate of CIG J0218.3-0510 corresponds to a large gravitational potential well. If this is the case, then the hot diffuse gas of the ICM should emit significant X-ray luminosity. This is supported by the X-ray detection we infer at the location of CIG J0218.3-0510 in § 2.6. Assuming that all the detected X-ray emission originates from the ICM we infer a mean temperature of ≈ 3 keV and virial mass of $1.1 \times 10^{14} M_{\odot}$ based on the local luminosity–temperature and mass–temperature relations (Arnaud & Evrard 1999; Arnaud et al. 2005). This is roughly a factor of 4 lower than the dynamical mass derived above, but within the large error budget. While the X-ray detection of CIG J0218.3-0510 supports the high derived virial mass, obtaining much deeper X-ray data is required for a self-contained analysis of the ICM properties and mass determination.

5. SUMMARY

We report the discovery of a spectroscopically confirmed galaxy cluster at $z=1.62$ located in the SWIRE XMM-LSS field. This cluster candidate was selected solely as an overdensity of sources with red *Spitzer*/IRAC colors, satisfying $([3.6]-[4.5])_{AB} > -0.1$ mag, with no other selection criteria imposed. Photometric redshifts derived from SXDS (*BViz*-bands), UKIDSS-UDS (*JK*-bands), and SpUDS (3.6-8.0 micron) for the galaxies in and around this cluster show that this structure corresponds to a galaxy surface density of sources at $z = 1.6$ that is $> 20\sigma$ times the mean surface density at this redshift. Furthermore, our recent analysis of existing *XMM* data on this cluster provides a weak but unambiguous detection compatible with the expected thermal emission from such a cluster. This confirms that our selection of overdensities of sources with red IRAC colors identifies galaxy clusters at $z \geq 1.3$.

We obtained spectroscopic observations of galaxies in the cluster region using IMACS on the Magellan telescope. We measured redshifts for five galaxies in the range $z=1.62-1.63$, all within 1.4 arcmin (< 0.7 Mpc) of the cluster center. In addition, we measured spectroscopic redshifts for two sources with $z=1.62-1.63$ within 1.4–2.8 arcmin (0.7–1.4 Mpc). The cluster appears to be dominated by red galaxies, with $(z-J) > 1.7$ mag. The photometric redshift distributions for the brightest red galaxies are centrally peaked at $z = 1.62$, coincident with the spectroscopically confirmed galaxies.

The $z-J$ versus J color–magnitude diagram of the galaxies in this cluster shows a strong red-sequence, which includes the dominant population of red galaxies. The rest-frame ($U-B$) color and scatter of galaxies on the red-sequence are

consistent with a mean luminosity–weighted age of 1.0–1.3 Gyr, yielding a formation redshift $\bar{z}_f = 2.35 \pm 0.10$, and corresponding to the last major episode of star formation in these galaxies.

We provide a crude estimate of the dynamical mass of CIG J0218.3-0510, although this result is highly uncertain due to systematics in the data and owing to the unknown dynamical state of CIG J0218.3-0510. Under the assumption that the dark matter halo of CIG J0218.3-0510 is virialized and relaxed, we estimate a dynamical mass based on the measured velocity dispersion, $M_{\text{dyn}} \sim 4 \times 10^{14} M_{\odot}$ within a virial radius of $r_{\text{vir}} \sim 0.9$ Mpc. Our reanalysis of the *XMM* X-ray emission of this cluster favors a lower virial mass, $1.1 \times 10^{14} M_{\odot}$, but consistent within the uncertainties. If these masses are accurate, then we expect CIG J0218.3-0510 to evolve to a rich cluster with $M \sim 10^{15} M_{\odot}$ at $z = 0.2$ similar to the Coma cluster. Further spectroscopic and multiwavelength observations of galaxies in CIG J0218.3-0510 are needed to constrain better the mass measurement.

We acknowledge our colleagues for stimulating discussions, and helpful comments. In particular, we wish to thank Chris Simpson and Masayuki Akiyama for their spectroscopic redshifts in advance of publication. We thank Renbin Yan for assistance with the spectroscopic reductions. We also acknowledge Stefano Andreon, Chris Simpson, S. Adam Stanford, and Jon Willis for very helpful feedback and suggestions. Lastly, we thank the anonymous referee whose helpful comments improved both the quality and clarity of this paper. This work is based on observations made with the *Spitzer Space Telescope*, which is operated by the Jet Propulsion Laboratory, California Institute of Technology. This work is based in part on data obtained as part of the UKIRT Infrared Deep Sky Survey. A portion of the Magellan telescope time was granted by NOAO, through the Telescope System Instrumentation Program (TSIP). TSIP is funded by NSF. Support for M.B. was provided by the W. M. Keck Foundation. We acknowledge generous support from the Texas A&M University and the George P. and Cynthia Woods Institute for Fundamental Physics and Astronomy.

REFERENCES

- Andreon, S., Maughan, B., Trinchieri, G., & Kurk, J. 2009, *A&A*, 507, 147
 Aragon-Salamanca, A., Ellis, R. S., Couch, W. J., & Carter, D. 1993, *MNRAS*, 262, 764
 Arnaud, M., & Evrard, A. E. 1999, *MNRAS*, 305, 631
 Arnaud, M., Pointecouteau, E., & Pratt, G. W. 2005, *A&A*, 441, 893
 Bahcall, N. A., Ostriker, J. P., Perlmutter, S., & Steinhardt, P. J. 1999, *Science*, 284, 1481
 Beers, T. C., Flynn, K., & Gebhardt, K. 1990, *AJ*, 100, 32
 Blakeslee, J. P., et al. 2003, *ApJ*, 596, L143
 —. 2006, *ApJ*, 644, 30
 Borgani, S., et al. 2001, *ApJ*, 561, 13
 Bower, R. G., Lucey, J. R., & Ellis, R. S. 1992, *MNRAS*, 254, 601
 Brammer, G. B., van Dokkum, P. G., & Coppi, P. 2008, *ApJ*, 686, 1503
 Brodwin, M., Gonzalez, A. H., Moustakas, L. A., Eisenhardt, P. R., Stanford, S. A., Stern, D., & Brown, M. J. I. 2007, *ApJ*, 671, L93
 Brodwin, M., et al. 2006, *ApJ*, 651, 791
 Brunner, R. J., & Lubin, L. M. 2000, *AJ*, 120, 2851
 Bruzual, G., & Charlot, S. 2003, *MNRAS*, 344, 1000
 Carlberg, R. G., Yee, H. K. C., Ellingson, E., Abraham, R., Gravel, P., Morris, S., & Pritchett, C. J. 1996, *ApJ*, 462, 32
 Carlberg, R. G., et al. 1997, *ApJ*, 485, L13
 Chiaberge, M., Capetti, A., Macchetto, F. D., Rosati, P., Tozzi, P., & Tremblay, G. R. 2010, *ArXiv e-prints*
 De Lucia, G., & Blaizot, J. 2007, *MNRAS*, 375, 2

¹⁶ Here M_{200} is the mass of the dark matter halo within a spherical volume defined by radius r_{200} where the average density is 200 times the critical density at the observed redshift.

- De Lucia, G., et al. 2007, *MNRAS*, 374, 809
- de Propriis, R., Stanford, S. A., Eisenhardt, P. R., Dickinson, M., & Elston, R. 1999, *AJ*, 118, 719
- Dressler, A. 1980, *ApJ*, 236, 351
- Eisenhardt, P. R. M., et al. 2008, *ApJ*, 684, 905
- Eke, V. R., Cole, S., Frenk, C. S., & Patrick Henry, J. 1998, *MNRAS*, 298, 1145
- Ellis, R. S., Smail, I., Dressler, A., Couch, W. J., Oemler, Jr., A., Butcher, H., & Sharples, R. M. 1997, *ApJ*, 483, 582
- Fazio, G. G., et al. 2004, *ApJS*, 154, 10
- Finkelstein, S. L., Papovich, C., Giavalisco, M., Reddy, N. A., Ferguson, H. C., Koekemoer, A. M., & Dickinson, M. 2010, *ApJ*, submitted, arXiv:0912.1338
- Finoguenov, A., et al. 2010, *MNRAS*, in press, arXiv:0912.0039
- Furusawa, H., et al. 2008, *ApJS*, 176, 1
- Gladders, M. D., & Yee, H. K. C. 2005, *ApJS*, 157, 1
- Gladders, M. D., Yee, H. K. C., Majumdar, S., Barrientos, L. F., Hoekstra, H., Hall, P. B., & Infante, L. 2007, *ApJ*, 655, 128
- Glazebrook, K., & Bland-Hawthorn, J. 2001, *PASP*, 113, 197
- Haiman, Z., Mohr, J. J., & Holder, G. P. 2001, *ApJ*, 553, 545
- Halliday, C., et al. 2004, *A&A*, 427, 397
- Hilton, M., et al. 2009, *ApJ*, 697, 436
- Hopkins, A. M., & Beacom, J. F. 2006, *ApJ*, 651, 142
- Jee, M. J., et al. 2009, *ApJ*, 704, 672
- Johnson, H. L. 1966, *ARA&A*, 4, 193
- Kajisawa, M., Kodama, T., Tanaka, I., Yamada, T., & Bower, R. 2006, *MNRAS*, 371, 577
- Kodama, T., Tanaka, I., Kajisawa, M., Kurk, J., Venemans, B., De Breuck, C., Vernet, J., & Lidman, C. 2007, *MNRAS*, 377, 1717
- Kriek, M., et al. 2006, *ApJ*, 649, L71
- Kurk, J., et al. 2009, *A&A*, 504, 331
- Kurk, J. D., et al. 2000, *A&A*, 358, L1
- Lawrence, A., et al. 2007, *MNRAS*, 379, 1599
- Lidman, C., et al. 2008, *A&A*, 489, 981
- Lonsdale, C. J., et al. 2003, *PASP*, 115, 897
- McCarthy, P. J., et al. 2007, *ApJ*, 664, L17
- Mei, S., et al. 2009, *ApJ*, 690, 42
- Miley, G. K., et al. 2004, *Nature*, 427, 47
- Mullis, C. R., Rosati, P., Lamer, G., Böhringer, H., Schwöpe, A., Schuecker, P., & Fassbender, R. 2005, *ApJ*, 623, L85
- Muzzin, A., et al. 2009, *ApJ*, 698, 1934
- Oke, J. B., & Gunn, J. E. 1983, *ApJ*, 266, 713
- Pacaud, F., et al. 2007, *MNRAS*, 382, 1289
- Papovich, C. 2008, *ApJ*, 676, 206
- Papovich, C., et al. 2006, *ApJ*, 640, 92
- Pelló, R., et al. 2009, *A&A*, 508, 1173
- Pierre, M., et al. 2004, *Journal of Cosmology and Astro-Particle Physics*, 9, 11
- Rosati, P., Borgani, S., & Norman, C. 2002, *ARA&A*, 40, 539
- Rosati, P., et al. 2004, *AJ*, 127, 230
- . 2009, *A&A*, 508, 583
- Rudnick, G., et al. 2009, *ApJ*, 700, 1559
- Sawicki, M. 2002, *AJ*, 124, 3050
- Simpson, C., & Eisenhardt, P. 1999, *PASP*, 111, 691
- Simpson, C., et al. 2006, *MNRAS*, 372, 741
- Springel, V., et al. 2005, *Nature*, 435, 629
- Stanford, S. A., Eisenhardt, P. R., & Dickinson, M. 1998, *ApJ*, 492, 461
- Stanford, S. A., et al. 2005, *ApJ*, 634, L129
- . 2006, *ApJ*, 646, L13
- Steidel, C. C., Adelberger, K. L., Shapley, A. E., Erb, D. K., Reddy, N. A., & Pettini, M. 2005, *ApJ*, 626, 44
- Stern, D., Holden, B., Stanford, S. A., & Spinrad, H. 2003, *AJ*, 125, 2759
- Tanaka, M., Kodama, T., Kajisawa, M., Bower, R., Demarco, R., Finoguenov, A., Lidman, C., & Rosati, P. 2007, *MNRAS*, 377, 1206
- Tran, K., Franx, M., Illingworth, G. D., van Dokkum, P., Kelson, D. D., Blakeslee, J. P., & Postman, M. 2007, *ApJ*, 661, 750
- van Breukelen, C., et al. 2007, *MNRAS*, 382, 971
- . 2009, *MNRAS*, 395, 11
- van Dokkum, P. G., Franx, M., Fabricant, D., Illingworth, G. D., & Kelson, D. D. 2000, *ApJ*, 541, 95
- van Dokkum, P. G., Franx, M., Kelson, D. D., & Illingworth, G. D. 1998a, *ApJ*, 504, L17+
- van Dokkum, P. G., Franx, M., Kelson, D. D., Illingworth, G. D., Fisher, D., & Fabricant, D. 1998b, *ApJ*, 500, 714
- van Dokkum, P. G., & van der Marel, R. P. 2007, *ApJ*, 655, 30
- Venemans, B. P., et al. 2007, *A&A*, 461, 823
- Visvanathan, N., & Sandage, A. 1977, *ApJ*, 216, 214
- Werner, M. W., et al. 2004, *ApJS*, 154, 1
- Williams, R. J., Quadri, R. F., Franx, M., van Dokkum, P., & Labbé, I. 2009, *ApJ*, 691, 1879
- Wilson, G., et al. 2009, *ApJ*, 698, 1943
- Yamada, T., et al. 2005, *ApJ*, 634, 861
- Zirm, A. W., et al. 2008, *ApJ*, 680, 224